RECTIFIED ASTEROID ALBEDOS AND DIAMETERS FROM IRAS AND MSX PHOTOMETRY CATALOGS

ERIN LEE RYAN, CHARLES E. WOODWARD

Department of Astronomy, School of Physics and Astronomy, 116 Church Street, S. E.,

University of Minnesota, Minneapolis, MN 55455

ryan@astro.umn.edu, chelsea@astro.umn.edu

Received _____ ; accepted _____

ABSTRACT

Rectified diameters and albedo estimates of 1517 main belt asteroid selected from the IRAS and MSX asteroid photometry catalogues are derived from updated infrared thermal models, the Standard Thermal Model (STM) and the Near Earth Asteroid Thermal Model (NEATM), and Monte Carlo simulations, using new Minor Planet Center (MPC) compilations of absolute magnitudes (H-values) constrained by occultation and radar derived parameters. The NEATM approach produces a more robust estimate of albedos and diameters, yielding albedos of p_v(NEATM mean)= 0.081 ± 0.064. The asteroid beaming parameter (η) for the selected asteroids has a mean value of 1.07 ± 0.27, and the smooth distribution of η suggests that this parameter is independent of asteroid properties such as composition. No trends in η due to size-dependent rotation rates are evident. Comparison of derived η's as a function of taxonomic type indicates the beaming parameter values for S-type and C-type asteroids are identical within the standard deviation of the population of beaming parameters.

Subject headings: solar system: minor planets, asteroids: surveys

1.   INTRODUCTION

The study of planet building in protoplanetary disks is an emerging area of emphasis. The number of detected exoplanetary systems continues to increase (e.g., Bouchy et al. 2009; O'Toole et al. 2009) and the inventory of dust mineral composition, organic materials, water abundances, ices, and gas content in the planet forming regions is now routinely determined from remote sensing spectrophotometry obtained by the NASA *Spitzer* Space Telescope and other facilities. However, the process by which micron-sized dust grains, volatile ices, and gas coalesce, aggregate, and grow leading to large planet-sized bodies is not well understood. Within our solar system, the main belt and Near-Earth asteroids (NEAs), are relics from the epoch of planet-building (Bottke et al. 2005). These objects can be statistically surveyed to characterize the size-frequency distribution, related to the evolution of planetesimals the solar system, to determine the albedo distribution, a measure of compositional gradients extant at the epoch of planet building, and to constrain models of solar system evolution (e.g., Gomes et al. 2005).

However, models of solar system formation are primarily constrained by albedo calculations from the Infrared Astronomical Satellite (IRAS; Tedesco et al. 2002a) and the Mid-Course Satellite Experiment (MSX; Tedesco et al. 2002b) surveys. In this paper we re-analyze the asteroid photometry from IRAS and MSX with the Standard Thermal Model and the more recent Near Earth Asteroid Thermal Model to derive revised albedo and diameter estimates for asteroids detected in these surveys. We compare the results from our new analysis to occultation and radar derived diameters in an effort to assess which thermal model approach is of higher fidelity and therefore more applicable in the analysis of large volume ecliptic asteroid surveys such as those conducted by the NASA Wide-Field Infrared Satellite Explorer mission (WISE; Liu et al. 2008).

2. ARCHIVAL ANALYSIS

2.1. *Asteroid Selection from Catalogs*

The IRAS catalog was produced for asteroid sightings in IRAS survey data (Tedesco et al. 2004a). The flux catalog consists of 12, 25, 60, and 100 μm photometric data of varying qualities for 9244 asteroid sightings. In this catalog, the data quality flags (DQF) range from values of 1 (low-quality) to 5 (high-quality), the latter DQF value denoting asteroids detected a minimum of twice in a given IRAS photometric bandpass. We selected all asteroids from the IRAS catalog with a DQF value of 3 or greater, and with reported fluxes in either three or four IRAS bandpass for analysis. These selection criteria produce a catalog of 5940 sightings of 1425 individual asteroids.

The MSX sightings catalog (Tedesco et al. 2004b) contains 325 individual sightings of asteroids. Data quality from MSX is not flagged; therefore, our MSX selection criterion accepts all asteroids for which fluxes in either three or four bands are reported for a given single sighting. This results in a dataset of 185 sightings of 92 individual asteroids. Table 1, the criteria-selected asteroid catalog (CSAC), summarizes all asteroids extracted from the IRAS and MSX catalogs. The entire table is available in an one-line electronic compilation.

2.2. *Models*

To determine the albedos and diameters of asteroids present in IRAS and MSX data, we have utilized both the Standard Thermal Model (STM; Lebofsky & Spencer 1989) and the Near Earth Asteroid Thermal Model (NEATM; Harris 1998). We used these models to generate a best-fit spectral energy distribution (SED) from all flux measurements simultaneously obtained at a given epoch for each asteroid in our CSAC database. Our approach differs from the methodology employed by Tedesco et al. (2004a,b) where albedos

and diameters were determined in each observation band and then averaged for the reporting of a "bulk" albedo.

The STM and the NEATM commonly used to obtain diameters and albedos of asteroids from mid-infrared (IR) photometry incorporate a variety of assumptions, the validity of which can be tested given extensive and reliable observational data. Briefly, we highlight the assumptions of each model with particular emphasis on how model assumptions influence the derivation of diameters and albedos.

The STM (Lebofsky & Spencer 1989) is the model used for the analysis of IRAS data by Tedesco et al. (2004a). This model assumes that: an asteroid is a perfect sphere; the asteroid temperature distribution is function of angular distance from the sub-solar point; the IR flux scales linearly in magnitudes with phase angle; and the thermal flux from an asteroid only arises from the illuminated "day-side" of an asteroid. The STM also invokes use of a fixed parameter, η, referred to as the beaming parameter. The value of η is chosen such that the diameters of asteroids Ceres and Pallas derived from IR observations of (Lebofsky & Spencer 1989) are equivalent to those determined from stellar occultation experiments (i.e., direct measures). The η parameterization accounts for surface roughness and thermal inertia, tacitly assuming that all asteroids have a similar surface characteristics, and presupposes that all compositions have the same thermal inertia.

The thermal distribution assumed for the STM is defined as

$$T_{STM}(\Omega) = [\frac{(1-A)S_\odot}{0.756r_h^2\epsilon\sigma}]^{\frac{1}{4}} \times [cos(\Omega)]^{\frac{1}{4}} \tag{1}$$

where the temperature, T is in Kelvin, A is the geometric Bond albedo, $S_\odot$ is the solar constant (W m^{-2}), r_h is the heliocentric distance (AU), ϵ is the emissivity of the object (assumed to be 0.9), σ is the Stefan-Boltzmann constant, and Ω is the angular distance

from the sub-solar point.

Because the STM does not provide good fits to NEAs, Harris (1998) introduced the NEATM model. The NEATM assumes an asteroid is a perfect sphere, the temperature distribution on the asteroid is a function of both latitude and longitude, the asteroid has a spin axis perpendicular to the Sun-Earth plane, and only the "day-side" of the asteroid contributes to the thermal flux. This model does not scale the thermal flux as a function of phase angle, rather it numerically calculates the actual thermal flux detected from the illuminated portion of a smooth sphere visible at a given phase angle. The NEATM also utilizes a beaming parameter (η), but rather than treating it as a fixed value the model defines η as a measure of deviation from a smooth body with zero thermal inertia. As a free parameter, η is best-fit simultaneously with the geometric albedo of a target.

The object thermal distribution assumed for the NEATM is:

$$T_{NEATM}(\Omega) = [\frac{(1-A)S_\odot}{\eta r_h^2 \epsilon \sigma}]^{\frac{1}{4}}(cos\phi)^{\frac{1}{4}}(cos\theta)^{\frac{1}{4}} \qquad (2)$$

where ϕ is the latitude, and θ is longitude. All other variables in this relation are defined as in Eqn. 1.

Our implementation of the STM and the NEATM fits the observed photometric data using the downhill simplex method of chi-squared minimization (Press et al. 1993). The asteroid diameters are derived from the relation of Fowler & Chillemi (1992),

$$D(km) = \frac{1329}{\sqrt{p_v}}10^{\frac{-H}{5}} \qquad (3)$$

where p_v is the geometric albedo and H is asteroid absolute magnitude for both models.

Values for H are taken from the Minor Planet Center[1] (MPC). Many H-values have significantly changed and updates have been made to MPC compilations since the original dates of the IRAS and MSX publications (e.g., Table 1). Those objects detected with signal-to-noise ratios < 10 have their fluxes over predicted by the IRAS point source extraction routines (Tedesco et al. 2002a); however, these flux overestimates are linear with respect to signal-to-noise ratio and can be corrected with a multiplicative factor. The point source extracted fluxes (columns labeled "flux"), the multiplicative flux correction factor (columns labled "flux Correction"), and overestimate corrected fluxes (columns labeled "Corrected Flux") are reported in the CSAC.

We also utilize the color corrections published for IRAS and MSX (Beichman et al. 1988; Egan et al. 1999); these color corrections are calculated in 10 degree bins. We do not color correct the IRAS photometry based on the sub-solar temperature. Instead, we apply the color correction using the mean temperature of the illuminated face of the asteroid which allows the asteroid to have a non-zero thermal inertia (e.g., dependent on surface properties, rotational periods). The effective blackbody temperature of the asteroid SEDs utilizing the IRAS fluxes for a given sighting are cooler (i.e., the SEDs peak near 25 μm) than that of the sub-solar temperature inferred for the effective heliocentric distance. Therefore, we calculate the mean temperature (from the temperature distribution defined in each model) as a proxy for the effective temperature of the object for the purposes of color correction. Use of the sub-solar temperature for the color correction is especially problematic for the NEATM fits to asteroid photometry, as the adoption of a sub-solar temperature for the color correction introduces a somewhat simplified first order assumption regarding the thermal inertia of the body (i.e., the body has zero thermal inertia such that it is in instantaneous equilibrium with the radiation field), and hence complicates interpretation of the derived

---

[1]www.cfa.harvard.edu/iau/mpc.html

values of η. Our approach is a departure from the Tedesco et al. (2004a,b) methodology results which utilize the sub-solar temperature for color corrections.

Table 2 reports example orbital parameters and fluxes utilized interatively in the thermal model fitting of IRAS data after: (1) flux overestimation corrections have been applied to IRAS point source fluxes (Table 1); and (2) mean temperature analysis (an intermediate interative modelling step) color corrections are applied to the observed fluxes. Geometric albedoes and diameters derived from using the mean temperature color corrected fluxes in each model are also provided in this table. Entries in Table 2 should enable corroboration of our methodology. The entire table is available in an one-line electronic compilation.

The χ^2 minimization fitting of the asteroid photometric data from the STM and the NEATM do not yield formal errors for each fit parameter. To determine the uncertainty of the albedo, diameter, and where applicable η derived from the models, a Monte Carlo code was utilized in conjunction with the observed photometry to create 100 synthetic asteroid sightings per sighting for each body in Table 1. The 100 synthetic sightings retained the orbital information such as heliocentric (r_h) and geocentric distance (Δ), but varied the photometric flux within the photometric uncertainties cited in each of the original source catalogs for a given asteroid. Results of our model fits with Monte Carlo simulation of the photometric uncertainty is presented in Table 3. This table contains both the STM and the NEATM albedo and diameter determinations for each sighting. In the solutions catalog entries for which the STM solutions did not converge are marked with a value of -1000.0 in the albedo, albedo error, diameter, and diameter error columns.

3.   RESULTS & DISCUSSION

Mean albedo and diameter values for asteroids from MSX and IRAS are reported in our ancillary on-line catalog, whose format and example entries are given in Table 4. All subsequent analysis, discussion, and conclusions in this manuscript are based on the data in Table 4. Comparison of our STM results with those in previously published studies (e.g., Tedesco et al. 2004a,b), indicate that the albedos obtained using an ensemble of four simultaneous measured photometric bands are systematically bluer than those determined from the mean of single channel (i.e., single photometric band) albedos. The offset between the mean single channel albedos and simultaneous ensemble albedos is 12% of as depicted in Fig. 1.

The NEATM fits of asteroid albedo yield an albedo distribution for the main belt asteroids that are redder and narrower than the solutions from the STM. This effect is illustrated in Fig. 2, a histogram distribution of the derived geometric albedos of each model. The mean albedo for asteroid NEATM fits is p_v(NEATM mean)$= 0.081 \pm 0.064$ while the mean albedo for the STM solutions is p_v(STM mean)$= 0.120 \pm 0.099$. Canonically, the mean albedo adopted for main belt asteroids is 0.11 (Parker et al. 2008; Yoshida & Nakamura 2007; Ivezić et al. 2001).

Comparison of the albedos we have derived for individual objects cataloged in both the IRAS and MSX databases, to those estimated through use of either the IRAS or MSX observations alone differ with a dispersion of $\sim 4\%$, Fig. 3. Though many asteroids have multiple IRAS sightings, most of these sightings are separated by minutes. This observational cadence does not allow one to obtain infrared light curves for asteroids whose rotational periods have timescales of hours to days. The majority of asteroids sighted in the MSX catalog have photometry for only a single sighting, thus the photometry of these targets is not as robust as the observations from IRAS. Shape and inhomogeneous

surface compositions as well as flux measurement errors could also account for the observed dispersion between the IRAS and MSX albedos.

3.1.   *Validation of Model Asteroid Diameters*

Independent best-fits SEDs generated using the STM and the NEATM to the identical asteroid photometric datasets can yield very disparate results for derived diameters and albedos. For example, the NEA 1627 Ivar was observed in the IR by Delbo et al. (2003). The solutions for this target using the STM and the NEATM yield geometric albedos ranging from 0.05 to 0.20, corresponding diameters between 9.12 km to 7.94 km respectively. The radar derived effective diameter (Ostro et al. 1990) of Ivar is 8.5 km.

The validity of thermal models fits to the IRAS photometric data of Tedesco et al. (2002a) is difficult to assess as the model-estimated diameters of Ceres are not equivalent to the occultation-derived determinations. This discrepancy is problematic as the STM model was optimized with a beaming parameter η set to 0.756 for the large asteroids Ceres and Pallas which may have thermal characteristics that are distinct from the general asteroid population (Lebofsky & Spencer 1989). The derived diameters for the largest asteroids observed by IRAS apparently are systematically low due to the use of "band-to-band" albedo corrections (Tedesco et al. 2002a). The band-to-band correction is a multiplicative factor of 1.12 which is applied to 25 and 60 μm derived albedos such that their values come into agreement with those albedos derived from 12 μm photometry.

Derivation of the band-to-band correction is not clearly explained in either Tedesco et al. (2002a), Tedesco et al. (1992), or Tedesco (1994), hence examination of the underlying assumptions (e.g., wavelength dependent η) and their overall validity is difficult. However, to test the general applicability of the Tedesco et al. (2002a) invoked

band-to-band corrections, we ran the STM on the single channel photometry at 12, 25 and 60 μm and determined the mean difference between occultation and radar derived diameters (many of which were not earlier extant) to those derived from IRAS data. In this analysis we utilized occultation and radar derived diameters of 80 asteroids and find the mean difference between the occultation-derived diameters and the 12 μm only diameters was $\simeq 17\%$, and $\simeq 25\%$ and $\simeq 5\%$ for the 25 and 60 μm only diameters, respectively. This analysis suggests that use of a single channel albedo correction has highest fidelity when applied to IRAS 60 μm photometry.

To determine which thermal model (either the NEATM or the STM) approach generates diameters that are commensurate with asteroid diameters determined by independent and/or direct measurement techniques, we have compared object diameters in Table 4 to those diameters established by radar or occultation observations. Cross-correlation of catalog entries in the IRAS, radar, and occultation databases yields 118 asteroids for this inter-comparison, Table 5. Generally, the STM underestimates asteroid diameters by $\sim 10\%$ when compared to radar and occultation derived estimates, while the NEATM underestimates diameters by $\sim 4\%$ as illustrated in Fig. 4. In absolute terms, application of the NEATM approach yields refined diameters commensurate with radar and occultation measurements, Fig. 5. However, there are moderate uncertainties ($\simeq 10\%$) in the formal error of the derived diameters quoted for many asteroids observed with either radar or occultation technique. Thus, application of either the STM or the NEATM approach to model IR asteroid photometry is reasonable with appropriate assumptions and caveats.

3.2.   *The beaming parameter, η*

The beaming parameter, η, within the main belt asteroids follows an approximate Gaussian distribution for the 1481 bodies in our sample population, Fig. 6. The cut-off in

the histogram distribution at values of $\eta = 0.75$ and $\eta = 2.75$ are artifacts due to truncation criteria set within our code. The mean η for asteroids is 1.07 ± 0.27 (exclusive of those within the histogram bins at 0.75 or 2.75). The smooth distribution of η suggests that the beaming parameter is independent of asteroid properties such as composition. Comparison of the derived asteroid beaming parameters as a function of De Meo et al. (2009) taxonomic type indicates that η for S-type and C-type asteroids are identical within the standard deviation of the population beaming parameters.

Delbo & Tanga (2009) assert, based on recent analysis of IRAS asteroid photometry, that the thermal inertia behavior of asteroids is a power-law function of diameter, with a break in the relationship occurring at size of ~ 100 km. Delbo & Tanga (2009) speculate that this change in functional behavior may be due to differing regolith properties of small versus large asteroids. If regolith properties are size-dependent, trends in model-derived η values should be apparent on our analysis. Figure 7 presents the beaming parameter fits as a function of asteroid diameter derived from the NEATM modeling. For diameters $\gtrsim 100$ km, η has a fairly narrow range of values, $1.5 \lesssim \eta \lesssim 0.8$. Asteroids with smaller diameters have a much greater range of η, and only asteroids with diameters less than ~ 100 km are values of η significantly greater than 1.6 frequently apparent. The latter trend is consistent with the thermal inertia behavior suggested by Delbo & Tanga (2009).

Whether or not the behavior of η as a function of asteroid diameter is solely dependent on size and therefore unique requires that affects of size-dependent rotation rates are minimal. Faster rotational periods also can give rise to increased η depending on the pole orientation. Figure 8 presents the period, diameter, η surface for all asteroids in our survey which have tabulated rotational periods in the catalog of Harris et al. (2008). There are no systematic trends or correlations between η values and rotation periods for a given diameter. Asteroids with high η values (> 2.0) are not required to be monoliths rather that

rubble piles.

The diameter discrepancies between the STM and the NEATM confirm that use of a fixed beaming parameter $\eta = 0.756$ in the STM is not valid, especially for those asteroids with diameters < 100 km. The diameters obtained by Delbo & Tanga (2009) are commensurate with those we have derived using the NEATM (Table 6). Hence the NEATM appears to be the preferable model to invoke to derive diameters from photometry.

3.3. *Sparse-Sampling Effects*

Our thermal model analysis of asteroid SEDs derived from simultaneous multi-band photometry enables quantitative assessment of the relative quality of albedo and diameter determined for asteroids that have only single photometric band (i.e., single-channel) measurements. Comparison of albedos derived solely from 12 μm photometry to those resulting from model fits to SEDs differ by $\simeq 6\%$, while the variance between 25 μm only albedo fits and SEDs estimates are $\lesssim 45\%$. This discrepancy between albedo solutions may account for the distinct differences in our derived diameters and albedos (Table 4) compared to those previously published in the literature (Tedesco et al. 2004a,b) even though a band-to-band correction of the order 12% was applied to the 25 and 60 μm derived albedos from Tedesco et al. (2002a). However, the 12 μm only albedo fits are in better consonance with those derived from the ensemble SED model-fits because the 12 μm bandpass from IRAS is narrower than the 25 μm bandpass. Although color corrections exist for all IRAS wavebands, constraining albedo by use of the 25 μm photometry is difficult as the bandpass is $\simeq 15$ μm wide, and many albedo solutions can fit this single photometric point.

Asteroid albedos derived from MSX photometry show no clear divergence between the albedos determined from 4-channel simultaneous photometry (SED modeling) and albedos

obtained using the 12 and 14 μm channels individually. However, use of either the shortest or longest wavelength photometry does produce discrepant albedo estimates: the 21 μm photometry yields a variance of $\approx 10\%$, while the 8 μm produces an incongruity of $\approx 54\%$ compared to the SED derived values. The large differences in the derived albedos using the 8 μm photometry is most likely due to solution ambiguities arising from the steepness of the greybody curve on the Wien side of the Planck flux distribution and the 20% photometric uncertainty of the reported 8 μm flux densities.

3.4. *Spectroscopic Type and Albedo*

Future all sky surveys, such as currently being conducted by the WISE mission or those planned by Pan-STARRS (Veres et al. 2009) or the Large Synoptic Survey Telescope (Jones et al. 2009), require a means to relate asteroid colors to albedos in order to assess the NEA size, population, and earth impact threat. In the optical, the precise correlation of albedo and (B-V) color is uncertain. Veeder & Tedesco (1992) find two loci in albedo vs. (B-V) color, one clustering near (albedo, B-V) = ($\approx 0.05, \approx 0.7$), the other near ($\approx 0.22, \approx 0.85$) which we can reproduce from asteroids albedos derived from our NEATM models and their corresponding (B-V) colors derived from catalog entries curated at the Planetary Data System[2] node (Lagerkvist et al. 1995). To break this degeneracy many of the newer asteroid surveys are expanding into the near-IR (e.g., Trilling et al. 2009; Ryan et al. 2009). The Bus-DeMeo taxonomy (De Meo et al. 2009) is the first system which extends asteroid taxonomy to the IR (out to 2 μm).

Inspection of the NEATM albedos for the Bus-DeMeo taxonomic types (Table 7) indicates that the S- and C-type complexes have relatively narrow ranges of albedo. The

---

[2]http://pds.nasa.gov/

NEATM albedo histogram distributions of asteroids with known Bus-DeMeo S-, C- and X-type classifications is presented in Fig. 9. The NEATM albedo values for these classes are lower in value than the STM derived albedos. The NEATM albedo range best-matches the spectroscopically inferred compositions of S- and C-class asteroids as suggested by laboratory albedo measurements of ordinary chondrite and carbonaceous chondrite materials (Piironen et al. 1998). Possibly, observations of asteroids in photometric bands akin to the Sloan Digital Sky Survey (SDSS; Parker et al. 2008) filter set, when extended into the near-IR, could provide a basic taxonomic classification of a newly discovered object reliable enough to obtain an asteroid diameter within $\sim 10\%$. However, the veracity of this assertion cannot be assessed as asteroids selected for our thermal analysis (Table 1) are sufficiently large enough in size that they would have saturated the SDSS images and are thus not present in their moving target catalog (Ivezić et al. 2002).

4. CONCLUSIONS

We have derived new asteroid diameters and albedo estimates utilizing 1517 objects selected from the IRAS and MSX asteroid catalogues using updated infrared thermal models, the STM and the NEATM. Spectral energy distributions using multi-band simultaneous infrared photometry and new values for asteroid absolute magnitudes (H-values) compiled in the MPC were fit and rectified using available occultation and radar derived diameters as constraints. Our model analysis suggests that the NEATM produces a more robust estimate of albedos and diameters. With the NEATM approach we find that the mean asteroid albedo is p_v(NEATM mean)$= 0.081 \pm 0.064$, suggesting that the canonical albedo adopted for main belt asteroids, 0.11,(Parker et al. 2008; Yoshida & Nakamura 2007; Ivezić et al. 2001) may be an overestimate. The mean beaming parameter, η, of asteroids in our select compilation is 1.07 ± 0.27. The smooth distribution of η suggests that the beaming

parameter is independent of asteroid properties such as composition and no trends in η due to size-dependent rotation rates are evident. Comparison of the derived asteroid beaming parameters as a function of De Meo et al. (2009) taxonomic type indicates that η for S-type and C-type asteroids are identical within the standard deviation of the population beaming parameters.

Facilities: IRAS MSX

REFERENCES

Beichman, C, et al. (1988), Infrared Astronomical Satellite (IRAS) Catalogs and Atlases, vol. 1, Explanatory Supplement, 1988, ed. C. Beichman, et al., NASA RP-1190 (Washington, DC: GPO)

Bouchy, F., et al. 2009, A&A, 46, 527

Bottke, W. F., et al. 2005, Icarus, 179, 63

Delbó, M., Harris, A, W., Binzel, R. P., Pravec, P., & Davies, J. K. 2003, Icarus, 166, 116

Delbó, M., & Tanga, P. 2009, Planetary Space Sci., 57, 259

DeMeo, F., Binzel, R. P., Slivan, S. M, Bus, S. J., 2009, Icarus, 202, 160

Dunham, D. W., & Herald, D., 2009, Asteroid Occultations, EAR-A-3-RDR-OCCULTATIONS-V7.0. NASA Planetary Data System

Egan, M. P., Price, S. D., Moshir, M. M., Cohen, M., Tedesco, E., Murdock, T. L., Zweil, A., Burdick, S., Bonito, N., Gugliotti, G. M., & Duszlak, J., 1999, The Midcourse Space Experiment Point Source Catalog Version 1.2 Explanatory Guide, AFRL-VS-TR-1999-1522, Air Force Research Laboratory

Fowler, J. W. & Chillemi, J .R. 1992, IRAS asteroid data processing. In: Tedesco, E. F.,Veeder, G. J., Fowler, J. W., Chillemi, J. R. (eds.): The IRAS Minor Planet Survey. Technical Report PL-TR-92-2049, Phillips Laboratory, Hanscom AF Base, MA.

Gomes, R., Levison, H. F., Tsiganis, K. & Morbidelli, A. 2005, Nature, 435, 466

Harris, A. W., 1998, Icarus, 131, 291

Harris, A.W., Warner, B.D., and Pravec, P., Eds., Asteroid Lightcurve Derived Data V10.0. EAR-A-5-DDR-DERIVED-LIGHTCURVE-V10.0. NASA Planetary Data System.

Ivezić, Ž., et al. 2001, AJ, 122, 2749

Ivezić, Ž., Jurić, M., Lupton, R. H., Tabachnik, S., & Quinn, T. 2002, Proc. SPIE, 4836, 98

Jones, R. L., Chesley, S. R., Connolly, A. J., Harris, A. W., Ivezić, Ž., Knezević, Ž., Kubica, J., Milani, A. & Trilling, D. E. 2009, Earth, Moon, & Planets, 105, 111

Kaiser, N., et al., 2002, Proc. SPIE, 4836, 154

Lagerkvist, C. I., et al., 1995, Asteroid Photometric Catalog (3rd Update), EAR-A-3-DDR-APC-LIGHTCURVE-V1.0, NASA Planetary Data System

Lebofsky, L. A. & Spencer, J., 1989, in Asteroids II, eds. R. P. Binzel, T. Gehrels, and M. S. Matthews, (Univ. Arizona Press: Tucson), p. 128

Liu, F., Cutri, R., Greanias, G., Duval, V., Eisenhardt, P., Elwell, J., Heinrichsen, I., Howard, J., Irace, W., Mainzer, A., Razzaghi, A., Royer, D., Wright, E. L., 2008, Proc. SPIE, 7017, 15

Magri, C., Ostro, S.J., Rosema, K.D, Thomas, M.D., Mitchell, D.L., Campbell, D.B., Chandler, J.F., Shapiro, I.I., Giorgini, J.D., & Yeomans, D.K. 1999,Icarus, 140, 379

Magri, C., Nolan, M. C., Ostro, S. J., & Giorgini, J. D. 2007, Icarus, 186, 126

Ostro, S. J., Campbell, D. B., Hine, A. A., Shapiro, I. I., Chandler, J. F., Werner, C. L., & Rosema, K. D. 1990, AJ, 99, 2012

O'Toole, S. J., et al. 2009, ApJ, 701, 1732

Parker, A., Ivezic, Ž., Jurić, M., Lupton, R., Sekora, M. D., & Kowalski, A. 2008, Icarus, 198, 138

Piironen, J., Muinonen, K., Nousiainen, T., Sasse, C., Roth, S. & Peltoniemi, J. I. 1998, Planetary and Space Sci., 46, 937.

Press, W. H., Flannery, B. P., Teukolsky, S. A., Vetterling, W. T. 1993, Numerical Recipes in C, (Cambridge University Press: London)

Ryan, E. L., et al. 2009, AJ, 137, 5134

Shepard, M. K., Kressler, K. M., Ellen-Clark, B., Ockert-Bell, M. E., Nolan, M. C., Howell, E. S., Magri, C., Giorgini, J. D., Benner, L. A. H., Ostro, S. J. 2008, Icarus, 195, 220

Tedesco, E. F., Fowler, J. W., & Chester, T. J. 1992, IRAS asteroid data processing. In: Tedesco, E. F.,Veeder, G. J., Fowler, J. W., Chillemi, J. R. (eds.): The IRAS Minor Planet Survey. Technical Report PL-TR-92-2049, Phillips Laboratory, Hanscom AF Base, MA.

Tedesco, E. F. 1994, in Asteroids, Comets, Meteors 1993: Proceedings of the 160th International Astronomical Union, held in Belgirate, Italy, June 14-18, 1993, eds. A. Milani, M. Di Martino, and A. Cellino. Inter. Astronomical Union. Symp. No. 160, (Kluwer Academic Pub.: Dordrecht), p.55

Tedesco, E. F. et al., eds. 1995, UBV Mean Asteroid Colors, EAR-A-5-DDR-UBV-MEAN-VALUES-V1.2, NASA Planetary Data System

Tedesco, E. F., Noah, P. V., Noah, M., & Price, S. D. 2002a, AJ, 123, 1056

Tedesco, E. F., Egan, M. P., & Price, S. D. 2002b, AJ, 124, 583

Tedesco, E. F., Noah, P. V., Noah, M., & Price, S. D. 2004a, IRAS Minor Planet Survey, IRAS-A-FPA-3-RDR-IMPS-V6.0, NASA Planetary Data System

Tedesco, E. F., Egan, M. P., & Price, S. D. 2004b, MSX Infrared Minor Planet Survey, MSX-A-SPIRIT3-5-SBN0003-MIMPS-V1.0, NASA Planetary Data System

Trilling, D. E., et al. 2009, AAS/Division for Planetary Sciences Meeting Abstracts, 41, #43.02

Veeder, G. J. & Tedesco, E. F. 1992, IRAS asteroid data processing. In: Tedesco, E. F.,Veeder, G. J., Fowler, J. W., Chillemi, J. R. (eds.): The IRAS Minor Planet Survey. Technical Report PL-TR-92-2049, Phillips Laboratory, Hanscom AF Base, MA.

Vereš, P. Jedicke, R., Wainscoat, R., Granvik, M., Chesley, S., Abe, S., Denneau, L., & Grav, T. 2009, Icarus, 203, 472

Yoshida, F., & Nakamura, T. 2007, Planetary Space Sci., 55, 1113

This manuscript was prepared with the AAS LaTeX macros v5.2.

Table 1.   INPUT FLUXES FROM IRAS AND MSX

Source	Number	r_h	Δ	phase	H	G	wave1	flux1	flux1 Error	flux1 Correction	Corrected Flux 1	wave2	flux2	flux2 Error	flux2 Correction	Corrected Flux 2	wave3	flux3	flux3 Error	flux3 Correction	Corrected Flux 3	wave4	flux4	flux4 Error	flux4 Correction	C
		(AU)	(AU)	(deg)	(mag)		(μm)	(Jy)	(Jy)		(Jy)	(μm)	(Jy)	(Jy)		(Jy)	(μm)	(Jy)	(Jy)		(Jy)	(μm)	(Jy)	(Jy)		(
IRAS	1	2.951	2.769	20.030	3.340	0.120	12.000	374.673	36.116	1.000	374.673	25.000	642.159	70.440	1.000	642.159	60.000	333.461	59.195	1.000	333.461	100.000	119.630	20.849	1.000	
IRAS	1	2.951	2.768	20.030	3.340	0.120	12.000	312.981	30.129	1.000	312.981	25.000	628.203	68.761	1.000	628.203	60.000	297.782	39.112	1.000	297.782	100.000	108.973	20.317	1.000	

Table 2.   STM AND NEATM SOLUTIONS PER SIGHTING[a]

Asteroid Number	Heliocentric Distance (AU)	Geocentric Distance (AU)	Phase angle (deg)	H (mag)	G	STM 12 μm flux (Jy)	color 25 μm flux (Jy)	corrected 60 μm flux (Jy)	100 μm flux (Jy)	STM Geometric Albedo	results Diameter (km)	NEATM 12 μm flux (Jy)	Color 25 μm flux (Jy)	Corrected 60 μm flux (Jy)	100 μm flux (Jy)	NEATM Geometric Albedo	results Diameter (km)	Eta
3	2.170	1.700	27.070	5.330	0.320	108.471	173.577	64.128	28.960	0.219	244.172	104.856	177.392	64.721	28.960	0.189	262.797	1.039
3	2.124	1.442	24.620	5.330	0.320	104.259	175.596	60.516	30.225	0.194	259.323	101.898	179.372	61.627	30.225	0.191	261.275	0.895
4	2.569	2.153	22.310	3.200	0.320	183.566	422.888	129.028	64.33	0.342	520.367	183.566	422.888	129.028	64.330	0.348	515.855	0.842
5	2.252	2.111	-26.670	6.850	0.150	17.005	31.496	13.956	4.709	0.313	101.276	16.438	32.188	14.085	4.709	0.167	138.74	1.068
5	2.53	2.112	-26.670	6.850	0.150	16.714	29.834	13.630	4.215	0.317	100.658	16.157	30.490	13.756	4.215	0.190	130.021	0.954
5	2.252	2.110	-26.670	6.850	0.150	12.772	27.967	9.983	4.166	0.380	91.969	12.347	28.581	10.076	4.166	0.183	132.415	1.216
6	2.705	2.578	21.520	5.710	0.240	14.970	38.104	16.491	8.829	0.258	188.766	14.333	38.961	16.802	8.913	0.190	219.839	1.192
6	2.691	2.461	21.710	5.710	0.240	18.913	47.775	22.844	20.317	0.230	200.012	18.109	48.848	23.275	10.416	0.165	235.961	1.219

[a] Iterative estimates using mean temperature color color corrections derived from CSAC point source fluxes (Table 1) corrected for flux overestimation (see text §2.2)

Table 3.   MONTE CARLO STM AND NEATM SOLUTIONS PER SIGHTING

Asteriod Number	STM Albedo	STM Albedo Error (±)	STM Diameter (km)	STM Diameter Error (±km)	NEATM Albedo	NEATM Albedo Error (±)	NEATM Diameter (km)	NEATM Diameter Error (±km)	NEATM Eta	NEATM Eta Error (±)
1	0.086	0.004	973.048	24.100	0.097	0.004	91 4.344	19.653	0.750	0.000
1	0.095	0.004	926.012	19.380	0.108	0.004	8 70.222	17.316	0.750	0.000
1	0.093	0.004	935.983	21.892	0.105	0.005	8 79.717	21.693	0.750	0.000

Table 4. MEAN ALBEDO CATALOG FOR IRAS AND MSX ASTEROIDS

Asteroid Number	Source	Number STM Obs.	STM Albedo	STM Albedo Error (±)	STM Diameter (km)	STM Diameter Error (±km)	Number NEATM Obs.	NEATM Albedo	NEATM Albedo Error (±)	NEATM Diameter (km)	NEATM Diameter Error (±km)	NEATM Eta	NEATM Eta Error (±)
1	IRAS	6	0.120	0.019	855.463	56.960	6	0.104	0.006	886.476	27.304	0.852	0.102
2	IRAS	7	0.175	0.015	479.812	20.180	7	0.145	0.011	523.982	20.833	0.860	0.050
3	IRAS	8	0.213	0.012	248.481	6.840	8	0.191	0.018	262.012	12.047	0.999	0.075
4	IRAS	1	0.342	0.012	520.367	6.840	1	0.348	0.026	515.855	19.247	0.842	0.039
5	IRAS	3	0.337	0.026	97.968	3.623	3	0.180	0.017	133.726	6.468	1.079	0.094
6	IRAS	6	0.291	0.029	180.426	8.497	6	0.203	0.021	214.485	10.249	1.114	0.077

Table 5.   ASTEROID DIAMETERS FROM THERMAL MODEL, RADAR,
OCCULTATION MEASURES

Asteroid Number	STM Diameter (km)	NEATM Diameter (km)	Radar or Occultation Diameter (km)	Source Reference[a]
1	855.463± 56.960	886.476± 27.304	933.750± 4.789	1
2	479.812± 20.180	523.982± 20.833	539.700± 21.108	1
3	248.481± 6.840	262.012± 12.047	269.550± 2.460	1
4	520.367± 6.840	515.855± 19.247	505.000± 4.252	1
5	97.968± 3.623	133.726± 6.468	110.500± 5.423	1
8	115.773± 2.654	145.755± 7.060	162.350± 11.952	1
9	152.410± 0.008	178.112± 0.021	168.600± 2.786	1
13	223.078± 3.461	226.063± 9.485	203.400± 2.970	1
17	80.357± 3.299	95.846± 6.012	73.000± 4.072	1
20	152.266± 7.185	155.040± 9.617	145.000± 17.000	2
21	82.671± 2.568	104.214± 7.111	116.000± 17.000	2
23	101.978± 3.682	111.045± 6.269	106.000± 12.000	3
25	61.623± 2.017	83.388± 5.846	79.100± 1.414	1
31	265.939± 7.001	286.908± 12.536	280.000± 43.000	3
36	109.093± 2.852	121.072± 9.594	103.000± 11.000	3
39	155.123± 5.652	184.707± 10.567	181.150± 4.640	1
41	172.431± 4.078	207.867± 10.516	187.300± 6.220	1
47	107.752± 3.889	140.814± 6.580	138.000± 1.972	1

Table 5—Continued

Asteroid Number	STM Diameter (km)	NEATM Diameter (km)	Radar or Occultation Diameter (km)	Source Reference[a]
51	155.861± 3.982	164.416± 6.647	144.300± 2.746	1
52	264.319± 6.959	340.748± 13.370	319.200± 4.386	1
53	118.637± 3.549	115.306± 5.948	115.000± 14.000	3
54	177.420± 4.559	177.676± 7.551	147.550± 1.628	1
58	94.553± 3.113	102.704± 7.770	96.500± 23.000	1
60	63.131± 3.260	59.357± 2.991	60.000± 7.000	3
64	59.461± 3.927	83.146± 26.882	50.400± 2.202	1
66	70.440± 4.962	76.578± 4.826	69.000± 9.000	3
70	105.166± 2.797	130.885± 6.526	131.300± 1.082	1
74	127.668± 3.339	132.020± 5.322	97.900± 2.193	1
80	84.847± 2.109	81.149± 2.652	79.000± 10.000	2
83	79.310± 3.568	94.343± 5.319	84.000± 9.000	1
85	155.238± 5.089	168.014± 10.560	172.200± 17.576	1
88	207.877± 5.889	223.199± 10.219	207.550± 2.062	1
89	134.271± 4.003	160.839± 6.526	152.950± 8.424	1
94	183.167± 4.610	206.310± 8.974	189.600± 4.254	1
99	72.159± 3.668	78.009± 2.557	71.050± 1.063	1
101	57.216± 1.542	72.394± 3.267	66.000± 7.000	3

Table 5—Continued

Asteroid Number	STM Diameter (km)	NEATM Diameter (km)	Radar or Occultation Diameter (km)	Source Reference[a]
105	101.053± 2.806	120.572± 4.743	104.350± 3.680	1
106	127.316± 3.372	162.918± 7.857	148.600± 43.600	1
109	79.486± 2.420	111.367± 9.144	88.350± 1.166	1
111	140.163± 2.404	153.170± 5.790	131.400± 1.300	1
114	81.802± 2.106	103.009± 4.952	100.000± 14.000	3
116	75.953± 6.952	84.234± 6.884	82.900± 3.220	1
124	78.018± 2.375	75.021± 3.370	65.850± 2.508	1
134	122.953± 4.888	127.250± 6.227	115.050± 14.320	1
135	67.288± 1.886	92.128± 5.553	80.400± 1.838	1
137	129.284± 4.248	155.643± 10.656	144.000± 16.000	3
141	110.858± 3.263	139.842± 7.897	137.600± 10.610	1
144	138.402± 9.118	161.194± 9.020	143.475± 8.834	1
153	162.487± 6.247	177.424± 9.525	81.400± 7.301	1
182	36.815± 1.821	47.829± 3.720	44.000± 10.000	3
187	131.420± 4.659	132.073± 7.746	145.850± 2.766	1
192	90.305± 2.489	106.881± 4.972	98.350± 2.663	1
198	56.922± 3.630	64.951± 3.102	57.000± 8.000	3
200	125.108± 5.903	135.871± 6.905	128.250± 2.921	1

Table 5—Continued

Asteroid Number	STM Diameter (km)	NEATM Diameter (km)	Radar or Occultation Diameter (km)	Source Reference[a]
204	47.992± 2.399	54.150± 2.411	50.800± 1.300	1
208	42.340± 3.156	46.451± 4.140	44.400± 1.924	1
210	89.045± 8.350	85.968± 3.829	68.750± 0.781	1
211	142.574± 4.375	150.951± 7.501	143.000± 16.000	3
216	119.562± 3.205	140.736± 7.777	105.950± 8.964	1
225	121.595± 3.341	122.424± 5.788	118.150± 2.267	1
230	91.467± 1.890	118.601± 5.246	101.900± 8.028	1
238	149.208± 14.173	163.652± 7.149	146.750± 10.132	1
247	143.994± 3.901	156.694± 6.537	134.000± 15.000	3
248	52.534± 3.213	54.208± 2.683	54.250± 1.844	1
266	112.857± 2.781	125.199± 8.406	109.000± 15.000	3
279	134.096± 5.365	136.781± 7.105	124.450± 1.345	1
287	69.096± 1.788	68.111± 3.154	75.450± 2.309	1
306	48.239± 1.380	55.480± 2.810	52.250± 1.118	1
308	118.450± 4.131	162.260± 6.934	132.175± 33.037	1
313	100.619± 2.797	98.365± 4.106	96.000± 14.000	3
324	248.167± 8.809	239.982± 7.705	223.300± 7.839	1
334	151.454± 12.849	182.247± 19.883	174.300± 5.471	1

Table 5—Continued

Asteroid Number	STM Diameter (km)	NEATM Diameter (km)	Radar or Occultation Diameter (km)	Source Reference[a]
345	93.814± 5.894	106.199± 7.809	99.650± 0.990	1
350	109.823± 4.097	126.309± 6.137	99.800± 3.421	1
354	155.338± 5.161	165.204± 7.560	165.000± 18.000	3
372	192.825± 4.731	210.109± 9.500	195.150± 4.245	1
381	120.314± 3.447	136.567± 7.139	131.550± 2.025	1
386	145.672± 3.771	186.513± 9.510	176.800± 8.841	1
393	106.704± 26.987	109.777± 20.808	125.000± 20.000	3
404	98.447± 4.172	102.307± 4.536	100.200± 2.309	1
405	129.605± 3.970	134.897± 6.734	125.000± 16.000	3
409	139.102± 4.308	174.535± 7.395	165.150± 33.609	1
411	65.582± 2.218	84.158± 4.116	78.000± 1.556	1
419	106.639± 2.944	139.941± 5.967	126.800± 3.956	1
420	139.318± 6.006	160.326± 8.801	145.800± 1.924	1
429	61.054± 1.737	73.809± 3.548	70.000± 10.000	3
431	84.580± 2.590	102.113± 5.015	69.200± 5.883	!
444	159.343± 13.673	167.732± 6.772	169.150± 14.348	1
466	114.911± 3.557	131.924± 5.654	126.950± 4.000	1
471	121.829± 4.641	138.542± 6.229	130.900± 2.012	1

Table 5—Continued

Asteroid Number	STM Diameter (km)	NEATM Diameter (km)	Radar or Occultation Diameter (km)	Source Reference[a]
476	124.609± 4.018	124.022± 5.835	102.800± 10.265	1
488	155.986± 6.944	161.588± 7.390	150.000± 21.000	3
498	79.162± 3.536	90.904± 4.181	79.300± 2.961	1
522	104.419± 7.747	107.284± 9.370	89.300± 3.467	1
526	41.241± 7.747	46.173± 1.727	45.850± 1.030	1
530	77.184± 2.698	89.082± 5.887	88.250± 3.183	1
566	171.473± 1.191	190.084± 7.909	137.350± 13.741	1
568	84.541± 4.290	92.405± 4.763	76.250± 3.585	1
578	73.227± 2.549	72.777± 3.293	72.875± 6.395	1
580	42.101± 2.036	53.520± 2.705	49.800± 0.849	1
693	58.296± 1.784	77.257± 3.449	81.400± 1.200	1
697	70.259± 2.610	86.817± 3.948	75.300± 2.377	1
702	169.078± 4.344	215.635± 9.235	203.300± 4.188	1
704	285.197± 6.999	358.470± 14.745	329.950± 11.272	1
712	134.508± 3.720	141.183± 6.971	118.950± 2.476	1
747	159.136± 5.164	185.980± 10.415	182.450± 11.985	1
757	26.810± 1.222	39.395± 3.536	36.850± 1.432	1
790	165.446± 9.333	173.412± 7.380	153.350± 2.773	1

Table 5—Continued

Asteroid Number	STM Diameter (km)	NEATM Diameter (km)	Radar or Occultation Diameter (km)	Source Reference[a]
791	93.427± 2.834	115.038± 4.663	84.600± 4.386	1
828	47.734± 1.798	59.854± 3.655	51.500± 2.921	1
903	67.620± 3.070	69.855± 3.132	81.400± 1.200	1
914	66.960± 2.103	83.642± 3.762	91.450± 2.184	1
925	47.856± 1.551	63.805± 2.913	61.850± 1.887	1
976	82.830± 4.103	86.958± 5.074	67.400± 10.474	1
1263	51.232± 2.047	54.397± 2.722	45.050± 1.166	1
1409	36.294± 1.694	41.862± 2.747	81.400± 4.817	1
1512	79.277± 3.628	88.479± 4.289	67.500± 2.657	1
1867	111.352± 4.666	137.194± 3.874	127.300± 5.859	1

[a]Reference values correspond to the following papers: 1=Dunham & Herald (2009), 2=Magri et al. (1999), 3=Magri et al. (2007)

Table 6.   THERMAL MODEL DIAMETERS FROM STM, NEATM, and TPM[a]

Asteroid Number	Asteroid Name	TPM[a] Diameter (km)	STM Diameter (km)	NEATM Diameter (km)
21	Lutetia	107-114	82.67 ± 2.57	104.21 ±7.11
32	Pomona	84-86	80.73 ± 1.99	82.94 ±4.08
44	Nysa	80-82	71.95 ±2.14	76.50 ±3.83
110	Lydia	90-97	73.30 ±2.40	90.33 ±5.47
115	Thyra	90-94	66.70 ±1.66	83.02 ±4.86
277	Elvira	36-40	27.77 ± 1.24	33.98 ±1.97
306	Unitas	55-57	48.24 ±1.38	55.48 ±2.81
382	Dodona	74-76	49.02 ±1.83	68.66 ±3.86
694	Ekard	108-111	90.51 ± 4.34	101.87 ±17.15
720	Bohlinia	40-42	28.61 ± 0.98	40.21 ±3.13

[a]Thermal Physical Model of Delbo & Tanga (2009).

Table 7.   ALBEDO VALUES FOR DEMEO TAXONOMIC TYPES

Type	Number Objects of Type	STM Albedo	STM Albedo Range	NEATM Albedo	NEATM Albedo Range
S complex					
S	43	0.260	0.071	0.174	0.039
Sa	1	0.397		0.339	
Sq	4	0.258	0.031	0.213	0.064
Sr	2	0.219	0.029	0.167	0.029
C complex					
B	2	0.265	0.128	0.083	0.087
C	12	0.070	0.023	0.053	0.018
Cb	3	0.074	0.047	0.063	0.039
Cg	1	0.105		0.058	
Cgh	10	0.138	0.144	0.103	0.083
Ch	16	0.069	0.014	0.052	0.009

Table 7—Continued

Type	Number Objects of Type	STM Albedo	STM Albedo Range	NEATM Albedo	NEATM Albedo Range
			X complex		
X	3	0.100	0.066	0.077	0.054
Xc	3	0.200	0.121	0.137	0.065
Xe	3	0.159	0.009	0.128	0.019
Xk	16	0.177	0.102	0.113	0.054
			End Members		
D	11	0.082	0.031	0.067	0.029
K	12	0.163	0.073	0.116	0.042
L	12	0.141	0.037	0.110	0.035
T	4	0.054	0.013	0.042	0.005
A	4	0.265	0.117	0.179	0.035
R	1	0.507		0.411	
V	1	0.3742		0.348	
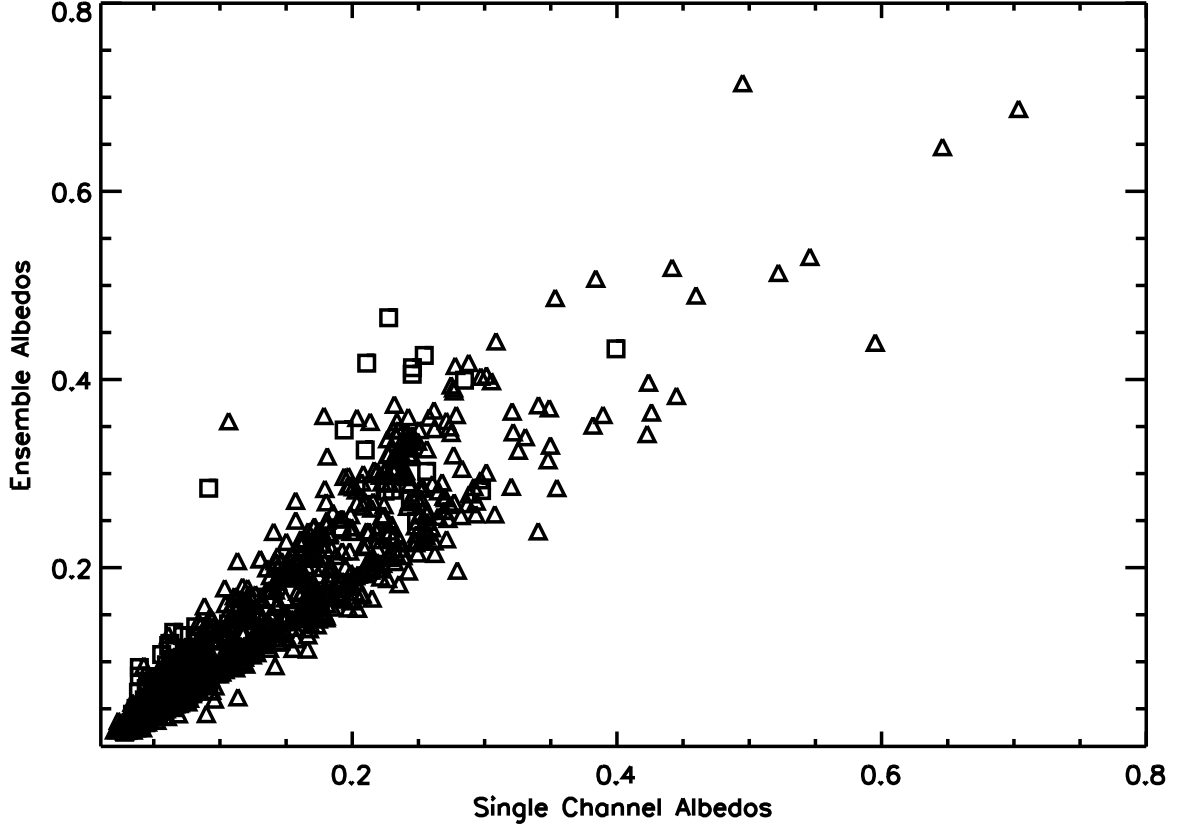
Fig. 1.— Mean single channel albedos versus newly recalculated mean ensemble albedos for IRAS and MSX sources summarized in Table 1. The *open triangles* correspond to IRAS sources, while *open squares* denote asteroids from the MSX catalogue. The correlation slope has a value of 1.10 for IRAS asteroids and 1.28 for MSX asteroids.
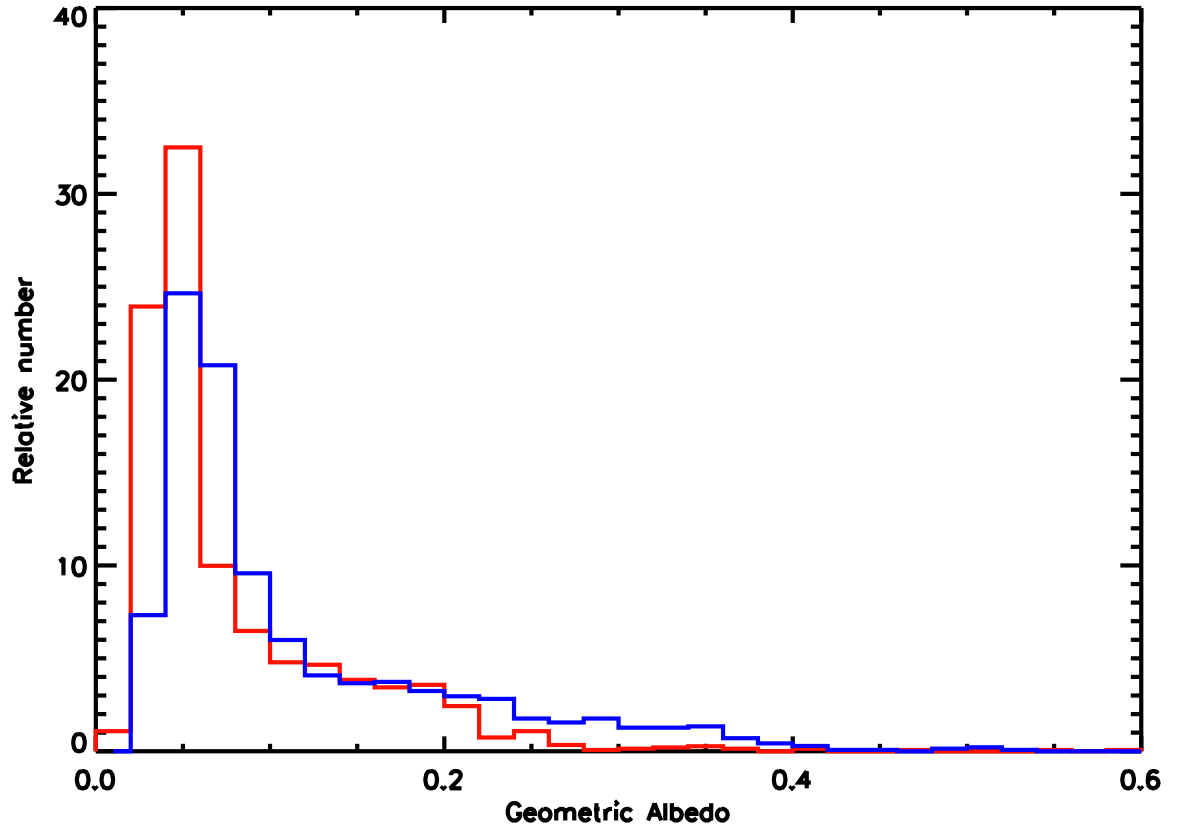
Fig. 2.— Histogram distribution of the NEATM and STM infrared thermal model albedos derived for asteroids culled from the original IRAS asteroid photometry catalog. The red line denotes the NEATM results, the blue line denotes the STM albedos.
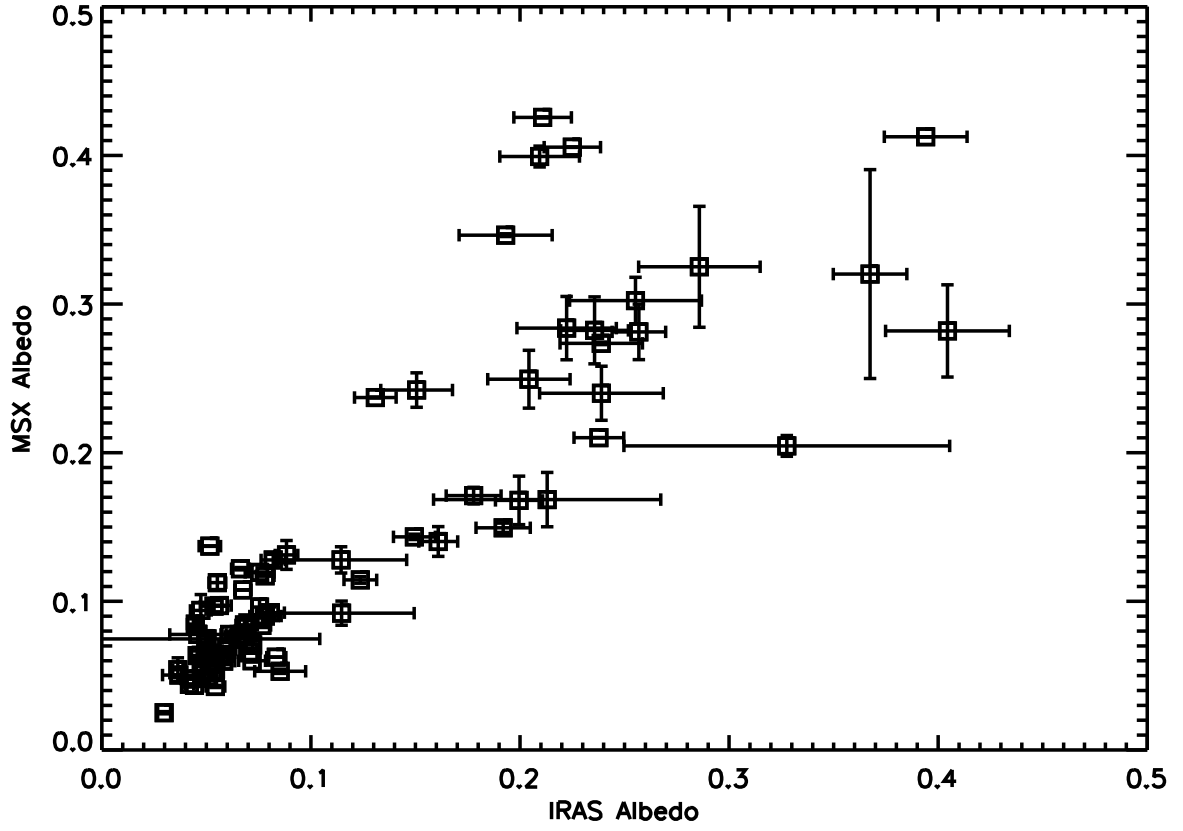
Fig. 3.— Comparison of asteroid albedos derived from IRAS photometry compared to those derived from MSX photometry of the same objects.
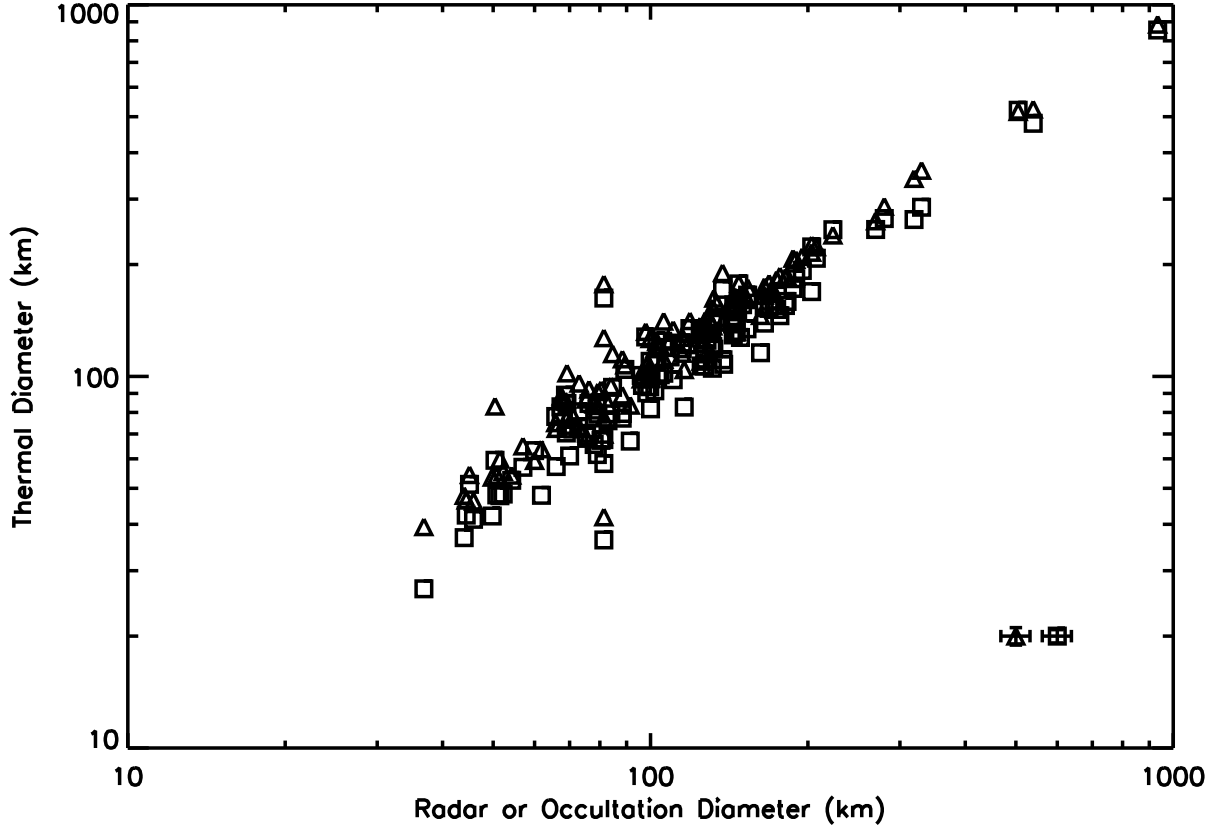
Fig. 4.— Asteroid diameters estimated from infrared thermal models versus diameters derived from either radar or stellar occultation experiments. *Open squares* denote diameters from STM calculations, while the *open triangles* denote diameters computed from NEATM models. The insert two symbols in the bottom right hand corner of the panel are indicative of the average diameter uncertainties for the thermal model diameters. The mean error for radar determined diameters is of order 6.4%.
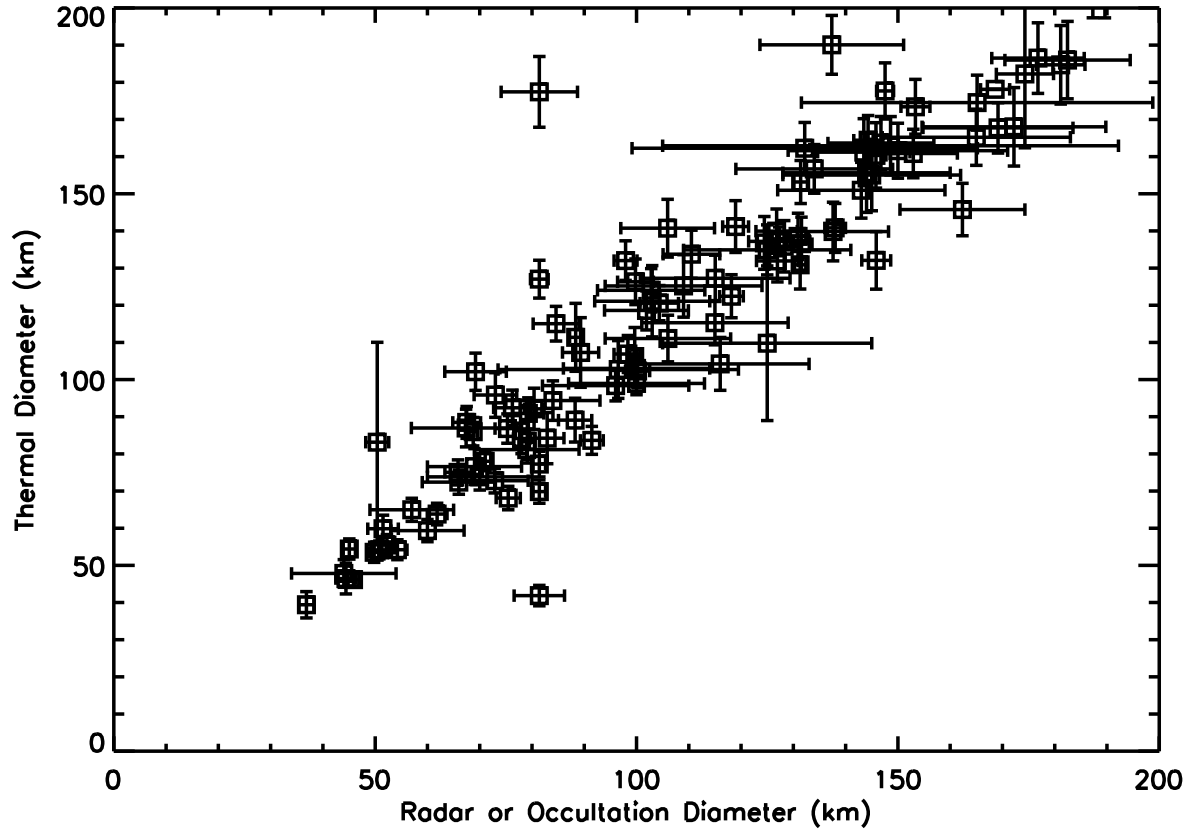
Fig. 5.— Correlation of NEATM derived asteroid diameters versus radar or occultation diameters.
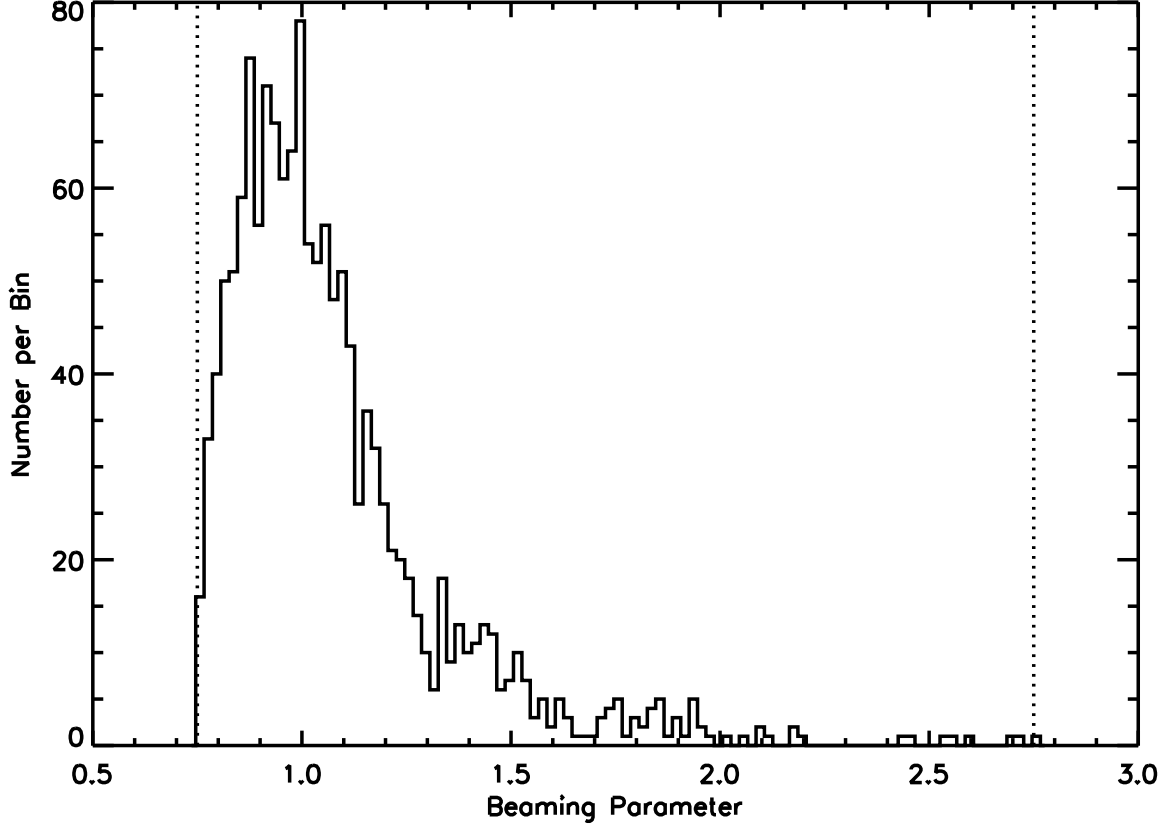
Fig. 6.— Histogram distribution of the derived beaming parameter, η, of main-belt asteroids from NEATM best-fit models to the spectral energy distribution assembled from IRAS and MSX photometry. The vertical dashed lines denoted limiting values set in the analysis code to force convergence.
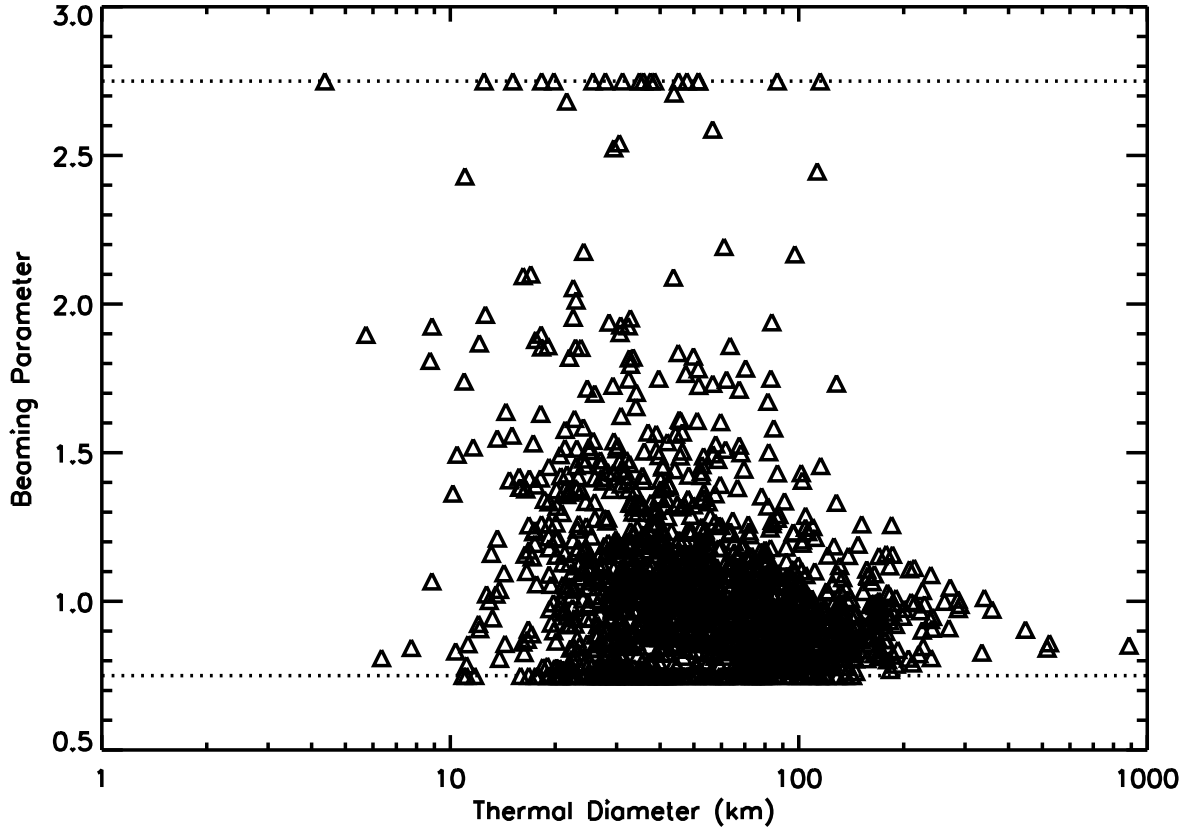
Fig. 7.— Derived beaming parameter, η, as a function asteroid diameter. The horizontal dotted lines are limits imposed in the modeling code to force convergence.
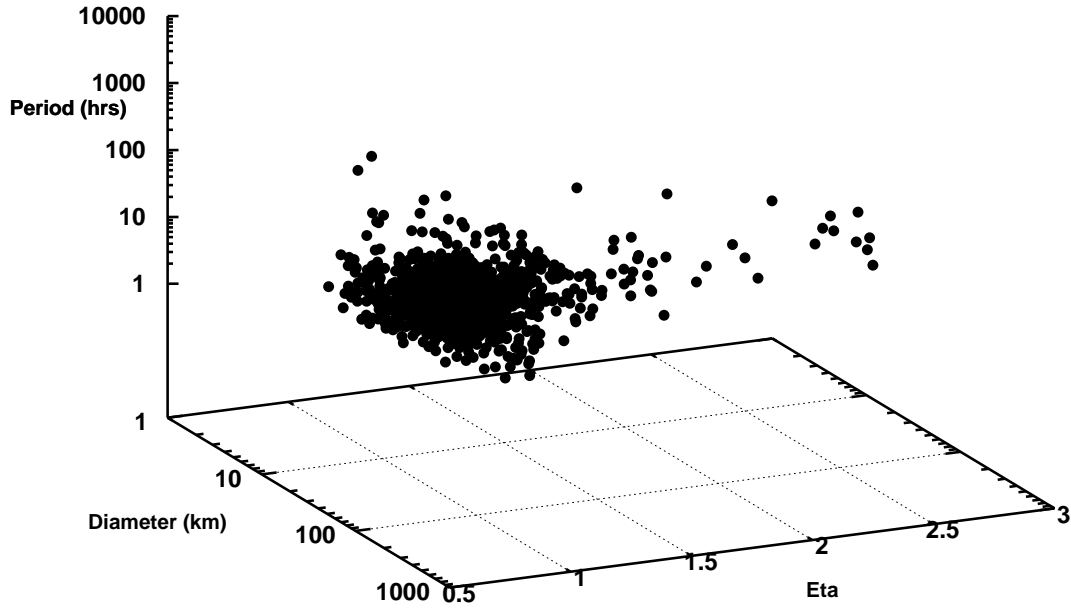
Fig. 8.— The rotational period, diameter, η phase-space for all asteroids within the study sample (Table 5) with known rotational rates as published in the catalog of Harris et al. (2008).
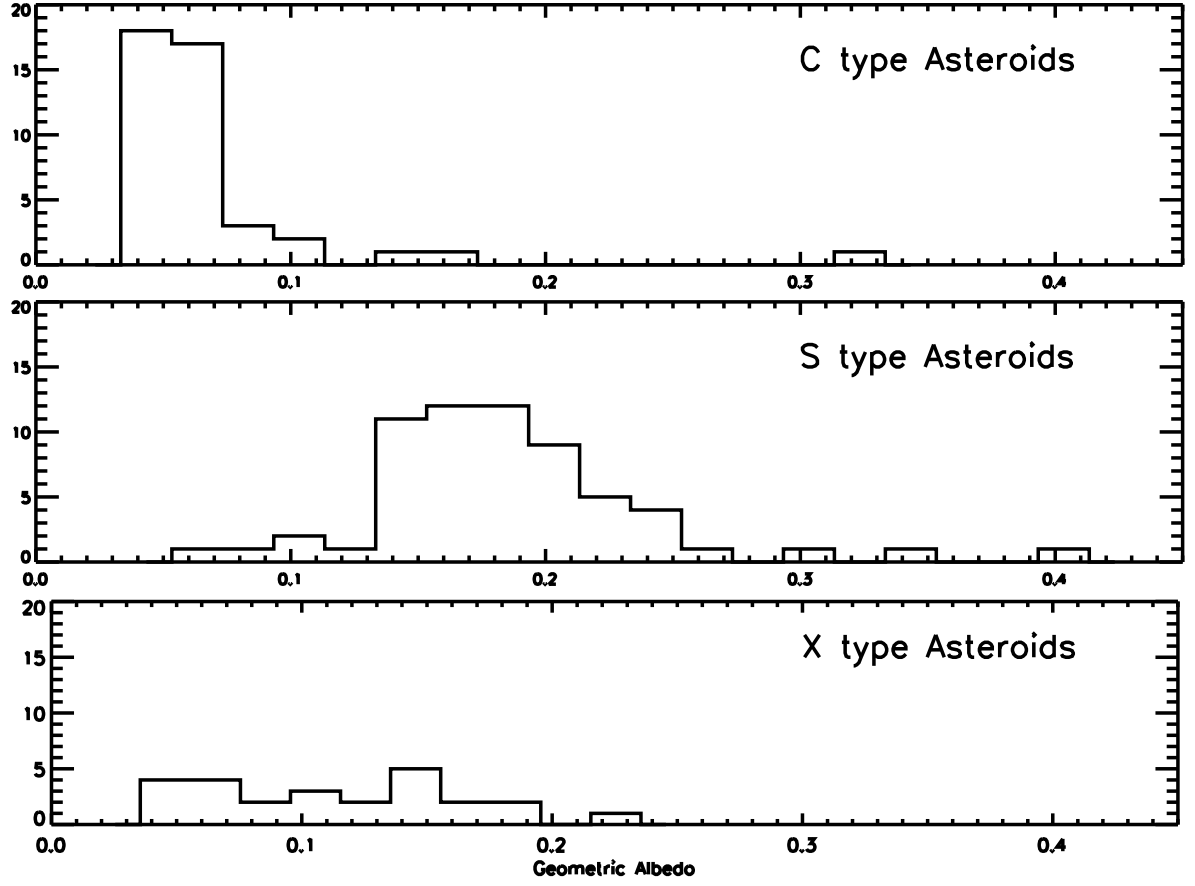
Fig. 9.— Histograms of asteroid NEATM albedos by taxonomic type, as defined by De Meo et al. (2009), for C-, S- and X-type classified asteroids in the study sample.